

Structure Evolution of a Polymer Solution at High Shear Rates

Kalman Migler,^{*,†} Chu-heng Liu,[‡] and D. J. Pine[§]Exxon Research and Engineering Company, 79 Route 22 East,
Annandale, New Jersey 08801Received July 13, 1995; Revised Manuscript Received November 27, 1995[®]

ABSTRACT: We utilized large angle light scattering to study the structure of a sheared semidilute polymer solution. Below a critical shear rate $\dot{\gamma}_c$ we observe an enhancement of concentration fluctuations in accordance with previous experimental and theoretical work. Above $\dot{\gamma}_c$ we find dramatic changes in the transient and steady state scattering behavior which indicate a shear-induced phase separation. A new four-peaked structure which coarsens in time is observed which is superimposed upon the scattering characteristic of low shear. The four-peaked scattering structure evolves into two peaks along the gradient direction, implying the formation of phase-separated domains elongated along the shear direction.

I. Introduction

Semidilute polymer solutions can undergo dramatic changes when subjected to shear or elongational flow fields.^{1,2} Transparent solutions, for example, can become cloudy and opaque to visible light for sufficiently strong flows. This cloudiness arises from a shear-induced enhancement of polymer concentration fluctuations and is largest in semidilute (*i.e.*, entangled) solutions near the Θ temperature; the magnitude of the effect increases as the coexistence (or binodal) phase boundary is approached. In some cases, phase separation and precipitation of polymer aggregates may occur.

Renewed interest in these phenomena has been stimulated by new theoretical models which attribute the shear-induced cloudiness to a coupling between flow-induced stress and thermally generated concentration fluctuations.^{3–7} Recent experimental work has focused on measuring the structure of the concentration fluctuations under shear flow.^{8–21} Reasonable agreement between theory and experiment has been achieved in the low to moderate shear regime. There is little understanding, however, of the solution behavior at high shear rates and, in particular, of questions regarding the possibility of shear-induced phase separation.

In this paper, we employ light scattering and rheological measurements to study the transient and steady state structures that are caused by the initiation of shear flow to a semidilute solution of polystyrene in dioctyl phthalate (DOP). Above a critical shear rate $\dot{\gamma}_c$, we observe qualitative changes in the structure factor, most notably the emergence of four new peaks which *coarsen* in time into two peaks along the gradient direction. Above $\dot{\gamma}_c$, we also observe a dramatic increase in the overall scattering amplitude. Other groups have observed dramatic increases in the scattering of either light¹⁵ or neutrons²⁰ above a critical shear rate under conditions similar to those reported here. Dramatic increases in the viscosity have also been reported above a critical shear rate.¹¹ The overall behavior of these experiments is suggestive of shear-induced phase separation.

In the present paper, we measure the static structure factor under shear flow in the shear plane and introduce a new analysis of the light scattering data in which the structure factor is decomposed into symmetric and antisymmetric components with respect to the shear flow. These two components exhibit vastly different dynamical behavior. The most important difference is that one component does not coarsen in time and resembles previously observed scattering patterns which are described by the HF model while the other component exhibits considerable coarsening behavior which occurs on relatively slow time scales and is not described by the HF model. The different dynamics of these two components suggests that the decomposition we employ has physical significance and may be able to provide guidance for the development of new theoretical models which can describe the high shear rate behavior of these polymer solutions. We critically discuss the implications of our results with respect to the suggestion that shear flow can induce some kind of phase separation. We also correlate our light scattering results with rheological data which show shear thinning and transient stress overshoots above $\dot{\gamma}_c$.

II. Background

Reports of shear-induced demixing in polymeric systems have appeared for over 30 years.¹ Only recently, however, has there been a significant effort to understand the physical origin of these phenomena and to develop a theory capable of quantitative explanations. In particular, experiment and theory have focused on understanding the structure of concentration fluctuations in sheared polymer solutions. Since the length scales of the concentration fluctuations enhanced by shear are comparable to the wavelength of light, light scattering techniques have proven to be useful probes. In a light scattering experiment, one measures the scattered light intensity as a function of scattering angle and obtains the static structure factor, $S(\mathbf{q})$. The static structure factor $S(\mathbf{q})$ is the Fourier transform of the spatial correlation function of the monomer concentration fluctuations,

$$S(\mathbf{q}) = V \int d\mathbf{r} \langle \delta c(\mathbf{r}) \delta c(\mathbf{0}) \rangle e^{-i\mathbf{q} \cdot \mathbf{r}} \quad (1)$$

Alternatively, one can measure the scattering dichroism which can be directly related to the second moments of $S(\mathbf{q})$.¹² Thus, one obtains the degree of anisotropy and orientation of $S(\mathbf{q})$.

[†] Present address: National Institute for Standards and Technology, Building 224, Room B210, Gaithersburg, MD 20899.

[‡] Present address: Wilson Center For Research & Technology, 800 Phillips Rd., Bldg. 128-33E, Xerox Corp., Webster, NY 14580.

[§] Present address: Department of Chemical Engineering, University of California, Santa Barbara, CA, 93106.

[®] Abstract published in *Advance ACS Abstracts*, January 15, 1996.

Simple shear flow determines a set of directions which can be used to define a coordinate system. We define x to be the flow direction, y to be the gradient direction, and z to be the vorticity direction. Thus, the flow field is completely specified by $v_x = \dot{\gamma}y$.

At low shear rates, Wu, Pine, and Dixon used a Couette flow cell to make angle-resolved light scattering measurements in the x - y plane.⁸ They found two peaks in the structure factor, that is, one peak at \mathbf{q}_{peak} and another at $-\mathbf{q}_{\text{peak}}$, as dictated by the symmetry of $S(\mathbf{q}) = S(-\mathbf{q})$. For low shear rates, the peaks are centered at angles of 45 and 225° from the q_x -axis. As the shear rate increases, the peaks rotate clockwise through the x -axis toward a limiting value of -45 and $+135$ °; scattering dichroism reveals behavior consistent with these observations.¹¹ A direct connection was made between the steady state shear-induced concentration fluctuations and the quiescent concentration fluctuations as measured by static and dynamic light scattering.⁹ The structures observed at low shear rates are in qualitative agreement with a model originally proposed by Helfand and Fredrickson (HF).³ Subsequently, Milner,⁴ Onuki,⁵ Doi,⁶ and Ji and Helfand⁷ extended the HF theory to account for various effects not considered in the original model. Within all of these models, thermal concentration fluctuations are enhanced by shear because of a coupling between the shear flow and concentration fields. The strength of this coupling is proportional to the concentration derivatives of the rheological transport coefficients, *i.e.*, proportional to $\partial\eta/\partial c$ and $\partial\Psi_1/\partial c$, where η is the viscosity, Ψ_1 is the first normal stress coefficient, and c is the polymer concentration. Within this general framework, peaks in the q_x - q_y plane are observed in the first and third quadrants at the lowest shear rates where the viscous shear stresses dominate (*i.e.*, the $\partial\eta/\partial c$ coupling). Empirically, this low-shear regime has been observed when the ratio of the normal to shear stresses is less than 0.2.⁸ At moderate shear rates, the two peaks move into the second and fourth quadrants where the normal stresses dominate (*i.e.*, the $\partial\Psi_1/\partial c$ coupling). This moderate-shear regime has been observed when the ratio of the normal to shear stresses is 2–5.^{8–12} Several groups have performed scattering experiments in the flow-vorticity plane (x - z).^{11,12,14–16,19,21}

At low to moderate shear rates, butterfly patterns are observed in which there is a “dark streak” along the vorticity direction. This behavior is similar to what has been predicted theoretically.⁷ At high shear rates numerous groups have reported dramatic results. Ver-Strate and Philippoff made the original observation of a sharp enhancement of turbidity above a critical shear rate,²² which has been more recently confirmed by both light scattering^{10–12,14–16} and neutron scattering^{19,20} studies. More importantly, these optical and neutron scattering studies have provided additional information about the structure of the polymer solutions above this critical shear rate. Light scattering studies show that the butterfly patterns persist out to high shear rates, with markedly increased intensity and a narrowing of the width of the dark streak. Nakatani *et al.*¹⁹ find a critical value of q above which fluctuations are not enhanced. For sufficiently large shear rates, some samples exhibit a shear thickening regime (following a shear thinning regime at moderate shear).^{10,11,15,17} During shear thickening, fluctuating rheological and light scattering signals are sometimes observed. Overshoots in various measurements such as scattering dichroism,

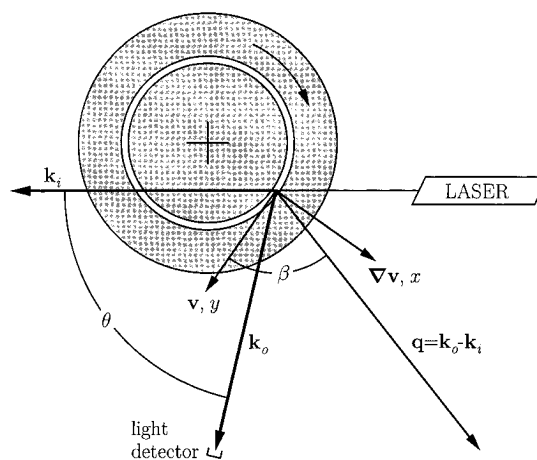


Figure 1. Schematic of the light scattering apparatus. The sample is contained in the gap between the inner and outer glass cylinders (shaded regions). The refractive index of the glass closely matches that of the sample, thereby minimizing refraction and reflection at the glass interfaces. The scattering angle θ is defined by the incident wavevector \mathbf{k}_i and scattered wavevector \mathbf{k}_o . The angle β is defined as the angle between the velocity vector \mathbf{v} and the scattering vector \mathbf{q} . The scattering volume is the volume of sample illuminated by the laser beam near the point where the vectors meet in the diagram. For the coordinate system we use, the velocity direction defines the x -axis and the gradient direction defines the y -axis.

birefringence, and stress have been reported upon initiation of strong shear flow.^{11–13,15,17} Yanase *et al.*¹¹ have observed that long times are required for the sample to reach equilibrium after cessation of shear flow. They have interpreted their high shear data in terms of a flow-induced phase separation.

III. Light Scattering Setup

We are interested in probing the concentration fluctuations which occur in the plane containing the flow (x) and gradient (y) directions. Because of the symmetry imposed by the shear flow, the leading order perturbations (proportional to $\dot{\gamma}$) of $S(\mathbf{q})$ must occur in the x - y (or q_x - q_y) plane. Higher order effects (proportional to $\dot{\gamma}^2$) will be manifest in both the x - y and x - z planes. We make measurements in the q_x - q_y plane by using a transparent glass shear cell, which is a modified version of the one presented in ref 9 (see Figure 1). The Couette cell consists of a stationary 23.4 mm diameter solid glass inner cylinder and a concentric cylindrical glass outer cup which rotates about the inner cylinder. The gap between the cylinders is 1.0 mm and contains the solution. Since the refractive index of the DOP solvent is 1.48 and the index of refraction of the Pyrex glass is 1.475, the reflection and refraction between the solution and the glass are minimized. Furthermore, the Couette cell is immersed in an index matching fluid, which eliminates reflection and refraction from the outer surfaces of the cup. Light from a He-Ne laser is weakly focused onto the gap between the cylinders in a direction perpendicular to the common axes of the cylinders, as shown in Figure 1. The scattered light is focused by a small-aperture lens onto a fiber optic cable which is connected to a photomultiplier tube. The scattering wavevector \mathbf{q} is defined by $\mathbf{q} = \mathbf{k}_o - \mathbf{k}_i$ where \mathbf{k}_o is the wavevector of the scattered light and \mathbf{k}_i is that of the incident light. In the present case of elastic light scattering, $k_i = k_o = 2\pi n/\lambda$, where λ is the wavelength of light in vacuum, and n is the index of refraction of the solvent. The magnitude of q is set by the scattering angle θ via $q = 2k_i \sin(\theta/2)$, as in typical light scattering

experiments. Scattered light is collected for angles ranging from $\theta = 20$ to 165° , allowing the static structure factor $S(q)$ to be measured for scattering vectors q between 5 and $30 \mu\text{m}^{-1}$. We control the direction of \mathbf{q} relative to the flow by rotating the entire Couette cell about the scattering volume, which varies the angle β . Note that there are three components which can rotate in this setup. The first component is the cup, which rotates about the inner cylinder and provides the shear flow. The second component is the light detection arm which can be rotated about an axis that passes through the scattering volume; this allows us to vary the scattering angle θ . The third component is the entire Couette cell which can be rotated about the scattering volume; this provides us the ability to vary β .

In order to study the time development of the structure factor following initiation of shear flow, we use the following procedure. We fix the magnitude and direction of the scattering vector \mathbf{q} by setting the angles θ and β to the desired values. Before shearing the sample, we measure the quiescent scattering intensity $I(\mathbf{q}, \dot{\gamma}=0, t=0)$. Then we apply a constant shear rate $\dot{\gamma}$ and measure the scattered intensity as a function of time. The time-dependent scattered intensity $I(\mathbf{q}, \dot{\gamma}, t)$ is measured and normalized to the quiescent scattering intensity, $I(\mathbf{q}, 0, 0)$. This is useful because $I(\mathbf{q}, \dot{\gamma}, t)/I(\mathbf{q}, 0, 0)$ is independent of the size of the scattering volume and allows comparison of results at different angles. At $T = 15^\circ$, $S(\mathbf{q}, 0, 0)$ is nearly constant over the range of q studied, so that $S(\mathbf{q}, \dot{\gamma}, t) \propto I(\mathbf{q}, \dot{\gamma}, t)/I(\mathbf{q}, 0, 0)$. Therefore, for the purposes of reporting data, the static structure factors we report are defined as

$$S(\mathbf{q}, \dot{\gamma}, t) \equiv I(\mathbf{q}, \dot{\gamma}, t)/I(\mathbf{q}, 0, 0) \quad (2)$$

Thus, the equilibrium static structure factor $S(\mathbf{q}, 0, 0) \equiv S(\mathbf{q})$ is defined to be unity. After a predetermined amount of time, usually several minutes, we stop the shear and wait for the system to relax back to equilibrium. We repeat this procedure for about 100 points in the q_x - q_y plane and thereby obtain separate data files for each value of \mathbf{q} . Combining the data, we construct a q_x - q_y plot of the structure factor at each time step following the initiation of shear. The apparatus is computer controlled and the above procedures are automated. In generating two-dimensional plots of $S(q_x, q_y)$, we use the symmetry condition $S(\mathbf{q}) = S(-\mathbf{q})$. This is important because it reduces the number of points at which we must acquire data and thus minimizes polymer degradation over the course of our experiments. At a few selected values of \mathbf{q} we measured $S(\mathbf{q})$ and $S(-\mathbf{q})$ and verified that they were equal to within the accuracy that our instrument allows. Because we map out $S(\mathbf{q})$ in a point by point fashion, the resolution of our measurements is relatively low. However, the structures that we observe are sufficiently broad in \mathbf{q} space that this procedure is able to capture the important trends. Finally, we note that in plotting the two-dimensional structure factor, we have used a procedure which interpolates between data points as an aid for visualizing the results.

IV. Sample

The system we study is polystyrene (PS) dissolved in dioctyl phthalate (DOP). This system has a Θ temperature of 22°C and phase separates below approximately 10°C , making it convenient for study near room temperature. The polystyrene was obtained from Pres-

sure Chemical²³ and has a relative molecular weight of 1.03×10^6 and a polydispersity of $M_w/M_n = 1.1$. The mass fraction of polymer is 4%. The experiments reported here were carried out at 15°C .

We monitored degradation of the sample by watching for decreases in the scattering intensity upon repeating certain experimental runs. Within the time scale of our longest runs (about 1 h), degradation was small. However, over the course of numerous runs, we did find degradation, and the sample was changed when the scattering intensity of a given experiment diminished by about 10%.

V. Rheology

When shear flow is initiated in an entangled polymeric liquid, the stress in the liquid initially increases. For sufficiently low shear rates $\dot{\gamma}$, the stress rises monotonically to its final steady state value. At higher shear rates, the stress typically overshoots its ultimate value before settling to its steady state stress. When the overshoot in the shear stress is accompanied by an overshoot in the normal stress, the overshoots are thought to be caused by chain stretching.²⁴ The cross-over between low and high shear rates can be characterized by the solution's Weissenberg number, $W \equiv \dot{\gamma}\tau_R$, where τ_R is the longest stress relaxation time. Operationally, W is typically taken to be unity at the lowest shear rate where a polymer solution shows significant shear thinning.

There are also reports of double overshoots in measured stresses upon application of shear flow.²⁵⁻²⁷ Systems which exhibit the second overshoot are generally near a phase boundary. In a recent study involving 2% PS in DOP of high molecular weight ($M_w = 2 \times 10^7$), the first overshoot occurs at strains of about 10-25 whereas the second overshoot occurs at strains of about 500. The magnitude of the second overshoot decreases strongly with increasing temperature.²⁸ Mani *et al.* studied a PS/PVME blend using a fluorescent technique which is sensitive to local mixing and observed a temporal correlation between a second overshoot and demixing.^{25,26}

The rheological measurements were carried out in a temperature-controlled cone and plate rheometer. In Figure 2a, we show the transient shear stress for our sample as a function of time upon initiation of shear flow for several different shear rates. In the solutions we study, a small (barely discernible) overshoot is first observed at $\dot{\gamma} = 60 \text{ s}^{-1}$; no overshoot is observed at lower shear rates (*e.g.* for $\dot{\gamma} = 30 \text{ s}^{-1}$, the stress rises monotonically). The overshoot becomes more pronounced with increasing shear rate and is plainly visible for $\dot{\gamma} = 90 \text{ s}^{-1}$. Figure 2b shows similar overshoot behavior for the first normal stress as a function of time, suggesting that there is some chain stretching. For the largest shear rate shown in Figure 2 ($\dot{\gamma} = 120 \text{ s}^{-1}$), the shear stress shows a second smaller overshoot with a minimum between the two overshoot peaks. The normal stress shows an overshoot followed by a broad shoulder.

In Figure 3a we show the steady state viscosity η and first normal stress coefficient Ψ_1 as a function of shear rate. Both transport coefficients exhibit significant shear thinning above $\dot{\gamma} \sim 100 \text{ s}^{-1}$. Thus, the characteristic stress relaxation time for these solutions is on the order of $\tau_R \sim 0.01 \text{ s}$. We do not observe shear thickening behavior in our sample for the shear rates studied, consistent with observations by Moldenaers *et*

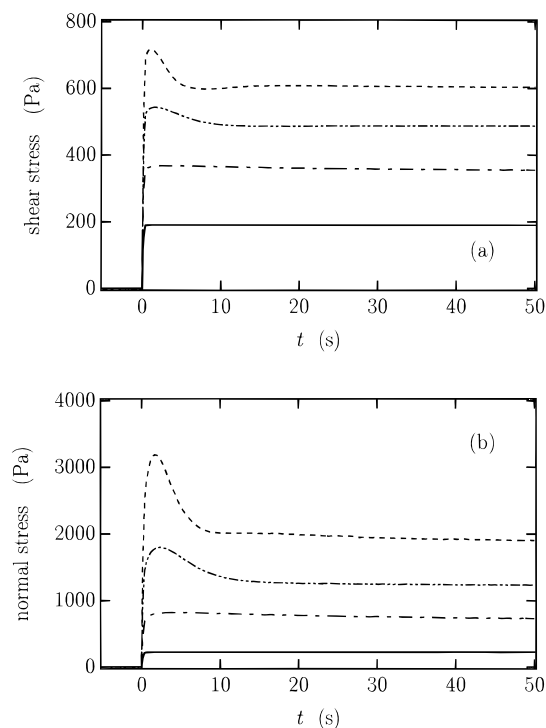


Figure 2. (a) Shear and (b) normal stress as a function of time after the initiation of shear flow for shear rates of 30, 60, 90, and 120 s^{-1} , in order, starting from the lowest curve in each plot.

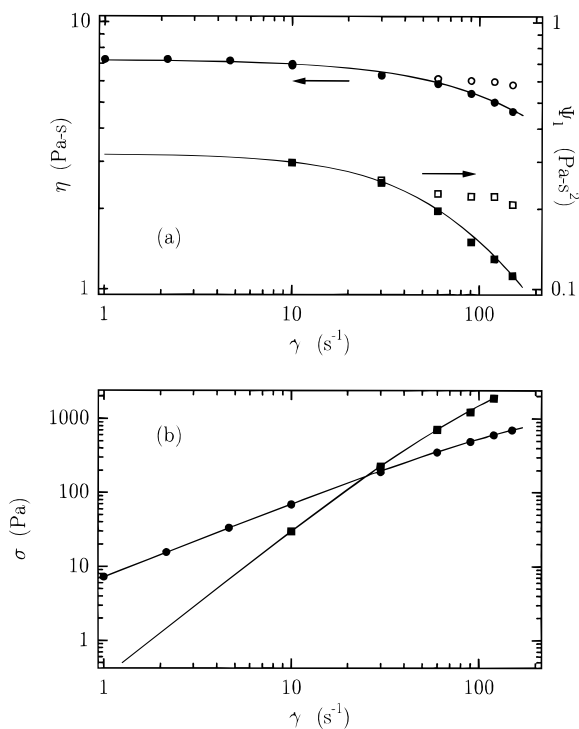


Figure 3. (a) Viscosity (circles) and first normal stress coefficient (squares) vs shear rate. The closed symbols are steady state values; the open symbols represent the peak values obtained during the transient startup. (b) Shear (circles) and normal stresses (squares) vs shear rate. Note that the normal stress exceeds the shear stress for shear rates greater than 25 s^{-1} . The solid lines through the data are only a guide for the eye.

*al.*¹⁰ In Figure 3a, we also plot the shear-rate dependence of the viscosity η and first normal stress coefficient Ψ_1 calculated from the measured peaks in the shear and normal stresses. These are nearly indepen-

dent of shear rate. The steady state shear and normal stress are plotted as a function of shear rate in Figure 3b. For $\dot{\gamma} < 25 \text{ s}^{-1}$, the shear stress is greater than the normal stress; for $\dot{\gamma} > 25 \text{ s}^{-1}$, the situation is reversed.

VI. Steady State Light Scattering Results

Profound changes in both the transient and steady state scattering patterns are observed as the shear rate exceeds $\dot{\gamma} \approx 60 \text{ s}^{-1}$. In Figure 4 we show the steady state structure factor $S(q_x, q_y, \dot{\gamma})$ for shear rates of 10, 30, and 60 s^{-1} . The contours in the figures indicate the enhancement in scattering arising from the imposed shear flow; a contour labeled “6” corresponds to a scattered intensity 6 times that of its equilibrium value.

Upon initiation of shear flow at these shear rates, $S(\mathbf{q})$ increases monotonically at all \mathbf{q} until the steady state is reached. This is consistent with results of experiments reported by van Egmond *et al.*¹² Our data indicate that there is a shear-induced enhancement in the amplitude of the naturally occurring concentration fluctuations in all directions and at all length scales probed in this experiment. A key qualitative feature of the plots in Figure 4 is the existence of the peaks at finite wavevector, which become more intense and rotate clockwise as the shear rate is increased. The existence of a peak in the scattering indicates that there is a particular wavelength and direction of strongest enhancement of the amplitude of the concentration fluctuations. For the data shown in Figure 4, the magnitude of the scattering vector at which the peak occurs in the same, within experimental uncertainty, for all three shear rates: $q_{\text{peak}} \approx 20 \mu\text{m}^{-1}$. The length scale associated with it is $2\pi/q_{\text{peak}} \approx 0.3 \mu\text{m}$. Previous experiments have shown that for low shear rates, the angle between the q_x -axis and the peak in the first quadrant is 45° and that as the shear rate increases, it rotates clockwise into the fourth quadrant.⁸ The rotation of the peak from the first to the fourth quadrants at moderate shear rates coincides with the normal stress dominating the shear stress. The rheological data in Figure 3b indicate that the normal stress equals the shear stress at $\dot{\gamma} \approx 25 \text{ s}^{-1}$ for our samples. The ratios of the normal to shear stresses for the shear rates of 10, 30, and 60 s^{-1} are 0.4, 1.2, and 2.0, respectively. Thus, from our discussion in section II, we expect the data for $\dot{\gamma} = 60 \text{ s}^{-1}$ to be in the “moderate” shear rate regime and the data at $\dot{\gamma} = 10$ and $\dot{\gamma} = 30 \text{ s}^{-1}$ to be intermediate between the “low” and “moderate” shear rate regimes. The data shown in Figure 4a,b, obtained at shear rates of 10 and 30 s^{-1} , exhibit peaks very near the q_x -axis; this is consistent with the shear and normal stresses making comparable contributions to the shear-enhanced (or stress-enhanced) light scattering. The data obtained at the higher shear rate of $\dot{\gamma} = 60 \text{ s}^{-1}$, shown in Figure 4c are in the normal-stress-dominated regime and exhibit peaks which have moved well into the second and fourth quadrants. These results are consistent with previous studies and with the modified HF model described in the background section.³⁻⁷

Our principle concern in this study is what happens to the scattering pattern as the shear rate is increased further. Figure 5 shows the steady state structure factor at shear rates of $\dot{\gamma} = 90 \text{ s}^{-1}$ and $\dot{\gamma} = 120 \text{ s}^{-1}$. Because we observed long-lived transients (discussed in the following sections), the sample was sheared for 1 h before taking data. The data show strong peaks near the q_y -axis at $q_{\text{peak}} \approx 10 \mu\text{m}^{-1}$ for $\dot{\gamma} = 90 \text{ s}^{-1}$ and at $q_{\text{peak}} \approx 5 \mu\text{m}^{-1}$ for $\dot{\gamma} = 120 \text{ s}^{-1}$. These peaks correspond to

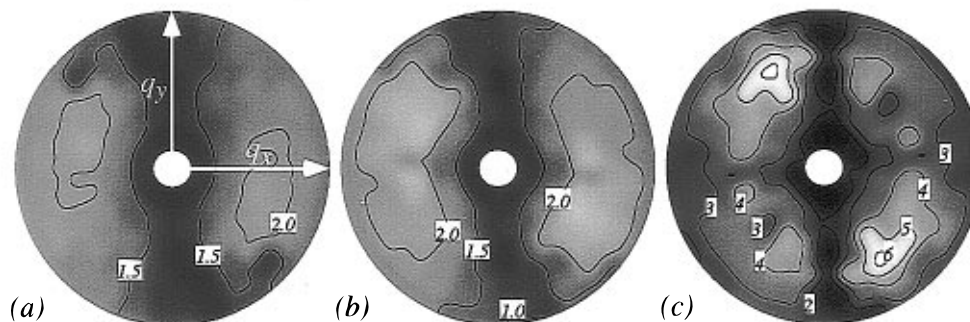


Figure 4. Steady state structure factor $S(q_x, q_y, \dot{\gamma})$ at (a) $\dot{\gamma} = 10 \text{ s}^{-1}$, (b) $\dot{\gamma} = 30 \text{ s}^{-1}$, and (c) $\dot{\gamma} = 60 \text{ s}^{-1}$. The contours indicate the enhancement in scattering arising from the imposed shear flow; a contour labeled “6” corresponds to a scattered intensity 6 times that of its equilibrium value. The gray scale in this and subsequent figures is a relative scale which is meant only to serve as a visualization aid.

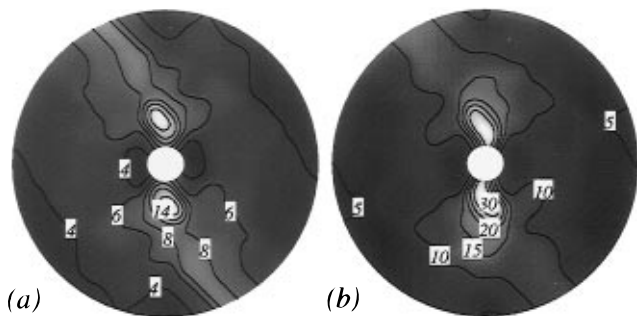


Figure 5. Steady state structure factor $S(q_x, q_y, \dot{\gamma})$ at (a) $\dot{\gamma} = 90 \text{ s}^{-1}$ and (b) $\dot{\gamma} = 120 \text{ s}^{-1}$.

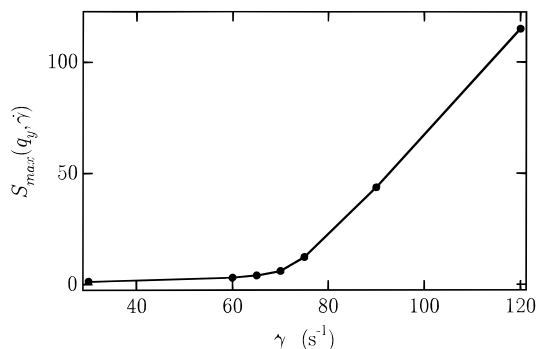


Figure 6. Maximum value of the structure factor at $t = 45 \text{ s}$ along the q_y -axis vs shear rate.

elongated concentration fluctuations which are oriented parallel to the flow (x) direction with a characteristic spacing along the gradient (y) direction of $2\pi/q_{\text{peak}} = 0.6 \mu\text{m}$ for $\dot{\gamma} = 90 \text{ s}^{-1}$ and $2\pi/q_{\text{peak}} = 1.3 \mu\text{m}$ for $\dot{\gamma} = 120 \text{ s}^{-1}$. The value of q_{peak} and its shear rate dependence for $\dot{\gamma} > 60 \text{ s}^{-1}$ is in striking contrast to the data for $\dot{\gamma} \lesssim 60 \text{ s}^{-1}$. Below 60 s^{-1} , the magnitude of q_{peak} is essentially independent of the shear rate, while above 60 s^{-1} , q_{peak} decreases dramatically with increasing shear rate. Typically, q_{peak} is 2–3 times smaller for $\dot{\gamma} \gtrsim 60 \text{ s}^{-1}$ than for $\dot{\gamma} \lesssim 60 \text{ s}^{-1}$. This indicates a coarsening in the characteristic length scale of the fluctuations by a factor of 2–3 for $\dot{\gamma} > 60 \text{ s}^{-1}$.

There are also other features in our light scattering data which indicate a qualitative change in the behavior of these solutions when the shear rate exceeds approximately 60 s^{-1} . First, the scattering intensity dramatically increases above $\dot{\gamma} \approx 60 \text{ s}^{-1}$. As one measure of this increased scattering, we plot in Figure 6 the *maximum* value of the structure factor at $t = 45 \text{ s}$ along the q_y -axis as a function of shear rate. Note the dramatic upturn in the scattering for $\dot{\gamma} > 60 \text{ s}^{-1}$.

Hashimoto and Kume¹⁵ have observed similar upturns in the scattering in the velocity–vorticity (x – z) plane above a critical shear rate (in what they call “Regime IV”). In addition, they note that these upturns are accompanied by dramatic changes in the light scattering pattern. In their light scattering patterns they observe a “dark streak” along the vorticity (z) axis which, for shear rates smaller than a critical shear rate, is rather broad and poorly defined. Above their critical shear rate the dark streak becomes much narrower and more sharply defined. This narrowing of the dark streak could coincide with the coarsening of the concentration fluctuations we observe in the x – y plane, though direct comparison between data sets is not possible given the difference in the molecular weights and concentrations of the samples.

Second, we observe an abrupt change in how quickly $S(\mathbf{q})$ decays after the shear flow is turned off. For $\dot{\gamma} \lesssim 60 \text{ s}^{-1}$, $S(\mathbf{q})$ decays to its equilibrium value more quickly than we are able to resolve, *i.e.*, in less than 1 s. By contrast, for $\dot{\gamma} > 60 \text{ s}^{-1}$, $S(\mathbf{q})$ typically takes 4–10 s to decay and can take as long as several minutes to decay depending on the value of \mathbf{q} (the relaxation after cessation behavior is discussed further in section VIIB). Thus, there appears to be a critical shear rate $\dot{\gamma}_c \sim 60 \text{ s}^{-1}$ above which our samples exhibit qualitatively different behavior, including a coarsening of the structures measured by light scattering, an increase in the light scattering intensity, and a dramatic increase in relaxation times. These observations are consistent with a growing body of experimental work in which dramatic increases in the scattering are observed above a critical shear rate.^{10–12,14–16,22} Nevertheless, these phenomena are still poorly understood.

What are the underlying causes of these changes? What are mechanisms which determine the length scale associated with q_{peak} and what determines how it changes with shear rate? To make progress toward answering these questions, we examine the temporal development of the light scattering patterns as they approach the steady state depicted in Figure 5.

VII. Transient Light Scattering Results

A. Commencement of Shear Flow. Upon commencement of strong shear flow ($\dot{\gamma} > \dot{\gamma}_c$), the evolution of the structure factor becomes rich and interesting. We can separate the transient response into two regimes. In the first regime, there is an overshoot in the scattering which essentially follows the overshoot observed in the rheological data. In the second regime, the scattering shows a coarsening behavior which occurs on longer time scales. In the second regime, the coarsening

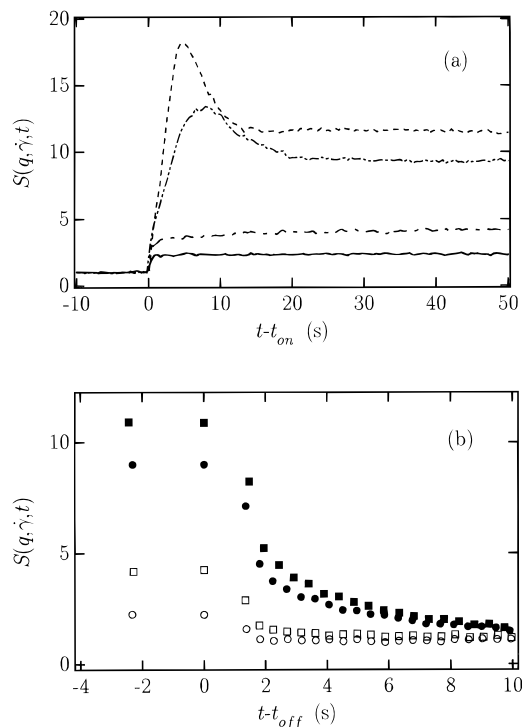


Figure 7. Light scattering upon (a) initiation and (b) cessation of shear flow for shear rates of 30, 60, 90, and 120 s^{-1} , in order, starting from the lowest curve in each plot. These data were taken at $q = 20 \mu m^{-1}$ and $\beta = 150^\circ$.

Table 1. Times of Peaks in Rheological and Light Scattering Data

	90 s^{-1}		120 s^{-1}	
	first peak	second peak	first peak	second peak
shear stress	1.5		1.1	8.0
normal stress	2.4		1.7	
light scattering	4.8		7.8	

observed suggests a phase separation driven by shear flow. While overshoots following the onset of shear flow have been observed in both mechanical and optical studies,^{11–13,15} the coarsening behavior at longer time scales has not been reported before.

The overshoot behavior is most conveniently observed by monitoring the scattered intensity as a function of time and shear rate at single points in q space. In Figure 7a we show the light scattering intensity as a function of time upon startup of shear. While these data are taken for the point $q = 20 \mu m^{-1}$, $\beta = 150^\circ$ ($q_x = -17.3 \mu m^{-1}$, $q_y = 6.8 \mu m^{-1}$), the trends shown in Figure 7a are common to most of q space. The data show a rapid increase in scattering immediately after the commencement of shear. One important feature is the strong influence in scattering when the shear rate exceeds 60 s^{-1} . Even more striking is the overshoot in the light scattering intensity, analogous to those in the rheological data for the higher shear rates. The shear rate at which overshoots occur in the light scattering corresponds very closely to the appearance of overshoots in the rheology, *i.e.*, at $\dot{\gamma} = 60 s^{-1}$. Moreover, the time after the initiation of shear flow at which the peak occurs decreases as the shear rate increases, just as for the rheological data. The light scattering peak, however, occurs slightly *after* the peak in the shear stress. Table 1 lists the times at which the various peaks in the rheological and light scattering data occur. Since a finite amount of time is required for the concentration

fluctuations to develop, it is reasonable to conclude that the peak in the light scattering represents the response of the concentration fluctuations to the prior peak in the stress (caused by chain stretching). This is consistent with the HF theory as modified by Milner⁴ to include the finite time it takes the concentration fluctuations to respond to the gradients in the stress field. Eventually, both the light scattering pattern and the stress settle into a steady state which does not decay with time.

While the above plots of particular values of q versus time are useful for observing the overshoot behavior, it is more useful to examine the full scattering pattern to visualize the coarsening behavior. In Figure 8a–d, we present the evolution of the structure factor for a shear rate of $\dot{\gamma} = 90 s^{-1}$, which is in the high shear rate regime. At very early times after the shear flow commences, we observe two peaks, one in the second and the other in the fourth quadrant, as shown in Figure 8a. The structure factor at this early time is qualitatively similar to the steady state structure factor seen previously at the shear rate of $\dot{\gamma} = 60 s^{-1}$ (see Figure 4c). Several seconds after the first two peaks appear, two new peaks emerge with one of the peaks in the first and the other in the third quadrant. They are 20%–30% less intense than the peaks in the second and fourth quadrants. All four peaks reach a maximum intensity after about 17 s (see Figure 8c) and then become less intense as $S(\mathbf{q})$ approaches its steady state configuration. Parts b–d of Figure 8 also show a coarsening of the structure. In Figure 8b, the position of the peaks occurs at $q = 20 \mu m^{-1}$, whereas in Figure 8d, it has moved to $q = 10 \mu m^{-1}$.

While the scattering patterns for $\dot{\gamma} = 90 s^{-1}$ shown in Figure 8b–d have four peaks instead of the two observed for $\dot{\gamma} = 60 s^{-1}$ in Figure 4, the patterns observed for $\dot{\gamma} = 90 s^{-1}$ exhibit the same underlying asymmetry as the one for $\dot{\gamma} = 60 s^{-1}$, namely, stronger scattering in the second and fourth quadrants than in the first and third quadrants. This asymmetry is an important feature of the original HF theory and has served to distinguish the HF mechanism from other proposed mechanisms.⁸ With this in mind, we decompose the scattering patterns for $\dot{\gamma} = 90 s^{-1}$ into two parts, one symmetric about the q_y -axis and the other antisymmetric about the q_y -axis. Our hope is that this will be useful for exploring the underlying mechanisms which drive the coarsening behavior. Thus, we write the structure factor as the sum of a symmetric component $S_s(\mathbf{q})$ and an antisymmetric component $S_a(\mathbf{q})$, that is,

$$S(\mathbf{q}) = S_s(\mathbf{q}) + S_a(\mathbf{q}) \quad (3)$$

with

$$S_s(\mathbf{q}) = \frac{1}{2}\{S(q_x, q_y) + S(q_x, -q_y)\} \quad (4)$$

and

$$S_a(\mathbf{q}) = \frac{1}{2}\{S(q_x, q_y) - S(q_x, -q_y)\} \quad (5)$$

We plot the antisymmetric component $S_a(\mathbf{q})$ in Figure 8e–h and the symmetric component $S_s(\mathbf{q})$ in Figure 8i–l for the same times that the full structure factor $S(\mathbf{q})$ is plotted in Figure 8a–d. Note that the antisymmetric component shows remarkably little evolution in time

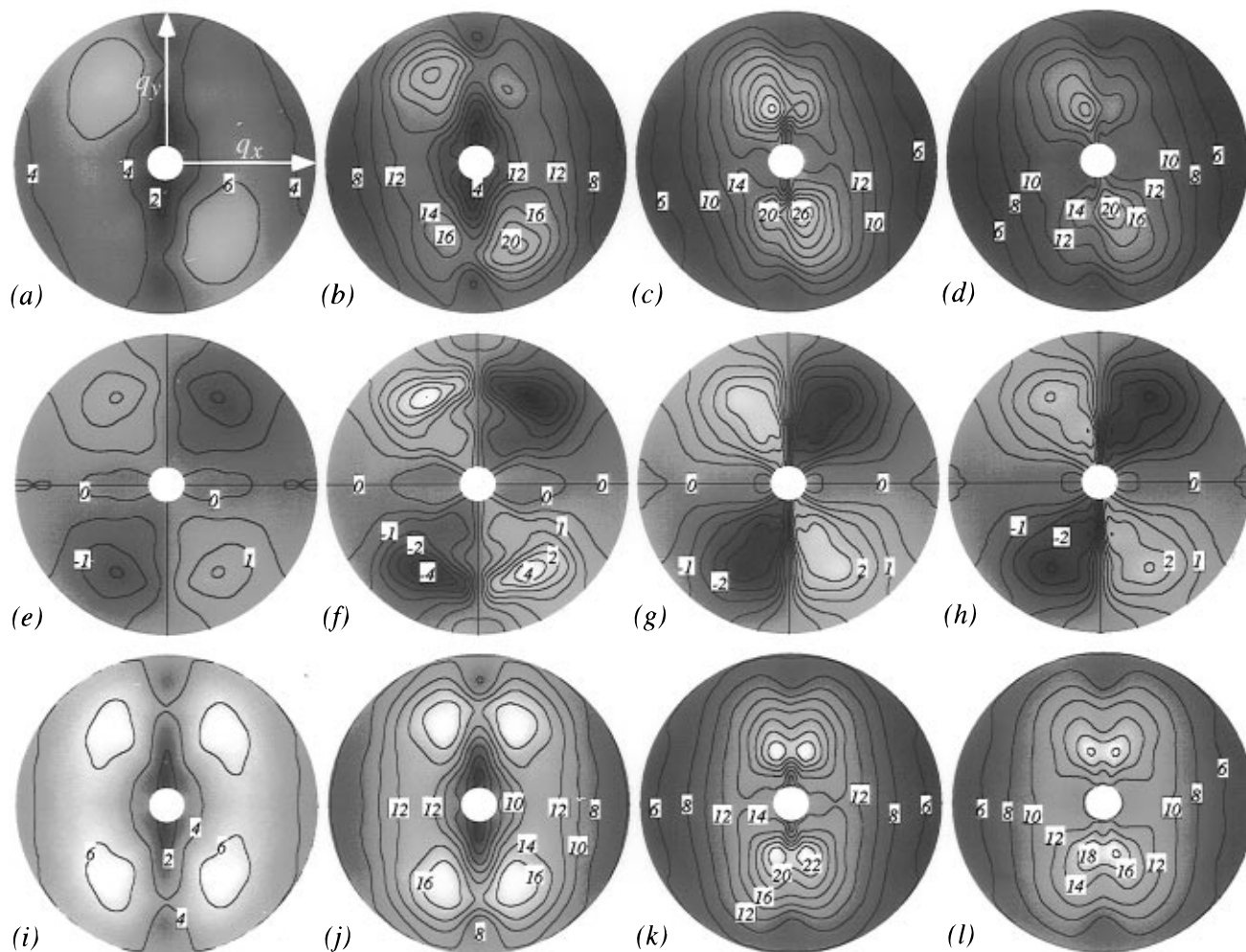


Figure 8. Evolution of the structure factor upon initiation of shear flow at $\dot{\gamma} = 90 \text{ s}^{-1}$. (a)–(d) The full structure factor, $S(q_x, q_y)$ at 2, 6, 17.5, and 45 s after the initiation of shear flow. (e)–(h) The antisymmetric part $S_a(q_x, q_y) = 1/2\{S(q_x, q_y) - S(q_x, -q_y)\}$ of the structure factors shown in (a)–(d). (i)–(l) The symmetric part $S_s(q_x, q_y) = 1/2\{S(q_x, q_y) + S(q_x, -q_y)\}$ of the structure factors shown in (a)–(d).

and, in particular, that the peaks observed in Figure 8h at $t = 45 \text{ s}$ are at essentially the same positions they were when they initially appeared at $t = 2 \text{ s}$, as shown in Figure 8e. In fact, the only significant time evolution in $S_a(\mathbf{q})$ occurs during the overshoot period occurring in the first 15 s after the initiation of shear flow. Moreover, there is no clear evidence of coarsening during this period; the changes in $S_a(\mathbf{q})$ are primarily changes in the intensity and not in the positions of the peaks.

By contrast, the symmetric component $S_s(\mathbf{q})$ shown in Figure 8i–l exhibits structures which continue to show significant evolution over a period 45 s or more. The most striking feature of $S_s(\mathbf{q})$ is the degree to which it coarsens over time. When the four symmetric peaks first appear several seconds after the initiation of shear flow, $q_{\text{peak}}^{(s)} = 20 \mu\text{m}^{-1}$; after 45 s the peaks have moved to $q_{\text{peak}}^{(s)} = 10 \mu\text{m}^{-1}$. The 4-fold peak structure observed in $S_s(\mathbf{q})$ coarsens by nearly a factor of 2 in the first minute after the initiation of shear flow.

The overall intensity of $S_a(\mathbf{q})$ is much weaker than that of $S_s(\mathbf{q})$. This indicates that the large enhancement in scattering that we are observing above $\dot{\gamma}$ is due primarily to the new symmetric mode. In fact, the overall intensity of $S_a(\mathbf{q})$ is comparable to the intensity seen at $\dot{\gamma} = 60 \text{ s}^{-1}$.

These observations that $S_a(\mathbf{q}, \dot{\gamma}, t)$ and $S_s(\mathbf{q}, \dot{\gamma}, t)$ develop on very different time scales and exhibit very different

scattering intensities are excellent indications that the mathematical decomposition we have performed has physical significance. Thus, it appears that in addition to the two-peak structure predicted by the modified HF theory, there is a new 4-fold symmetric mode in $S(\mathbf{q})$ which emerges at high shear rates and slowly coarsens over time. Patterns with a four-peak symmetry have been observed in extensional flow by van Egmond and Fuller.¹³ In their case, however, the pattern is symmetric with respect to the extensional axis, which is not the case for our study. Coarsening behavior was not reported, even for their highest strain rate, so it appears that the present experiment is probing a fundamentally different phenomenon.

The structure factor $S(\mathbf{q}, \dot{\gamma}, t)$ continues to develop, albeit slowly, on a time scale of longer than 5 min. In Figure 5a we show the steady state scattering pattern obtained after continuously shearing at $\dot{\gamma} = 90 \text{ s}^{-1}$ for 1 h. For various reasons, it is not feasible to obtain the full time dependence of the transient light scattering data over this entire period of time, so we just show the final steady state pattern. Nevertheless, we find that after shearing the sample for 1 h, the four-peak structure observed in the first minute after shearing has continued to develop in two significant ways: it has coarsened further and, where there once were four peaks, there are now only two which are clearly visible. Apparently, the two peaks in the first and second

quadrants have merged together to form a single peak along the y -axis; the peaks in the third and fourth quadrants have also merged in a similar fashion. In fact, if we return to Figure 8i–l, we find that the peaks in the first and second and in the third and fourth quadrants of the symmetric part of the structure factor are moving closer to each other and to the q_y -axis as time passes. Thus, we conclude that the two pairs of peaks initially observed in $S_s(\mathbf{q})$ do indeed merge into a single pair of peaks along the q_y -axis.

The enhanced scattering at small q near the q_y -axis corresponds to domains of enhanced polymer concentration which are strongly elongated after the flow direction. It is important to understand that in simple shear flow, structures which scatter along the q_y -axis possess a kind of stability or time independence which is not possible for structures which scatter in other directions. The key point is that fluctuations with nonzero q_x components are rotated and either stretched or compressed by shear flow. As a result, the value of \mathbf{q} for a given fluctuation changes in time according to the equation,

$$\mathbf{q}(t) = \mathbf{q}_0 - q_{x0}\dot{\gamma}t\hat{\mathbf{y}} \quad (6)$$

where \mathbf{q}_0 and q_{x0} are the initial values of the wavevector and its x component, respectively.³ This has the effect of limiting the growth in the size of fluctuations which have a finite q_x component. For example, consider the fluctuations shown in Figure 8 in the vicinity of the peak in the structure factor located at $(q_x, q_y) = (-5 \mu\text{m}^{-1}, 15 \mu\text{m}^{-1})$. Since the width Δq of the peak is approximately $5 \mu\text{m}^{-1}$, a fluctuation passing through this region of q space spends $\Delta t \approx \Delta q/q_{x0}\dot{\gamma}$ or approximately 0.01 s in this region of high growth for shear rates on the order of 100 s^{-1} . After this time, the fluctuation is convected to higher q values where the stress-induced enhancement mechanism is too weak to compete with diffusion and the fluctuation dies. Thus, the duration of time over which such a fluctuation can grow is limited by the finite amount of time it spends in the high-growth region of q space.

Fluctuations with $q_x = 0$ are unique, however, because they are not converted in a shear flow. This means that fluctuations near the q_y -axis can spend arbitrarily long periods of time in the high-growth region. Therefore, convection by the shear flow cannot prevent the amplitude of fluctuations near the q_y axis from growing to be quite large. Because of this property, it is useful to examine the time evolution of fluctuations along the q_y -axis in more detail. In Figure 9 we show $S(q, \dot{\gamma}, t)$ for a series of different times after the initiation of shear for $\dot{\gamma} = 90 \text{ s}^{-1}$. For clarity of presentation, the figure is broken into two parts: Figure 9a shows data for times less than 25 s and 9b shows data for times greater than 25 s. For $t < 25 \text{ s}$ (Figure 9a), the scattering increases with time for nearly all q_y . Soon after shear flow starts, a very broad peak in the scattering develops in the vicinity of $q_y \approx 15\text{--}25 \mu\text{m}^{-1}$. The peak becomes more pronounced with time and moves inward toward smaller q . For $t > 25 \text{ s}$ (Figure 9b), the scattering behavior is quite different: the scattering intensity generally gets weaker with time. The peak does continue to move inward toward smaller q_y . After several minutes, a steady state is reached with a peak in the vicinity of $5 \mu\text{m}^{-1}$. Presumably, this length scale is determined by a competition between the stress-induced growth forces which cause fluctuations to grow and diffusion which tends to dissipate and shrink fluctuations. As the shear

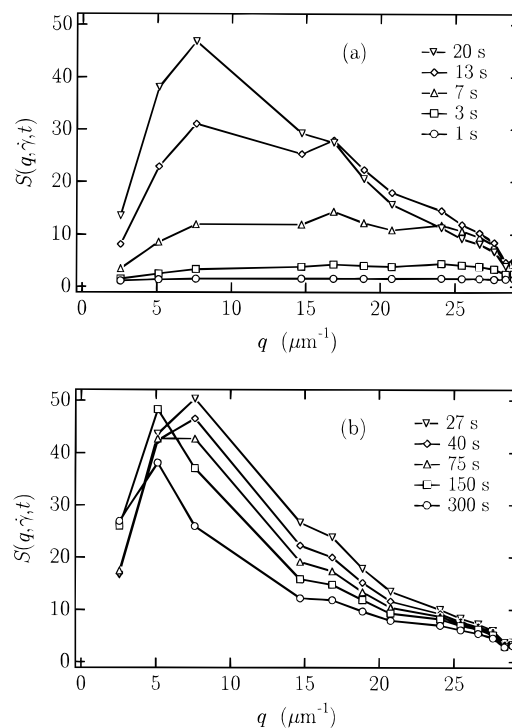


Figure 9. Evolution of $S(q, \dot{\gamma}, t)$ upon initiation of shear flow at $\dot{\gamma} = 90 \text{ s}^{-1}$ (a) for times less than 25 s and (b) for times greater than 25 s. The time for each curve is indicated in the plots.

rate is increased, the position of the peak moves toward smaller q_y . When the shear rate is increased beyond 120 s^{-1} , it moves to values of q_y too small for our instrument to resolve. Thus, it appears that the shear-induced coarsening mechanism dominates the forces which cause fluctuations to dissipate as the shear rate is increased.

B. Cessation of Shear Flow. In Figure 7b we show the scattered intensity as a function of time after the cessation of shear for four different shear rates: 30, 60, 90, and 120 s^{-1} . These data are taken for the point $q = 20 \mu\text{m}^{-1}$, $\beta = 150^\circ$ but show the trends that are common to most of q space. The most striking feature is that there is a dramatic increase in the relaxation time for $S(\mathbf{q}, \dot{\gamma}, t)$ when $\dot{\gamma}$ exceeds 60 s^{-1} . The fast relaxation time for the lower shear rates is consistent with our previous studies.⁹ The longer relaxation times of several seconds observed for the shear rates in excess of 60 s^{-1} are not at all consistent with this previous result and show that the system has been driven very far from its equilibrium state.

Before discussing the new data, it is useful to review the results of previous measurements of the relaxation dynamics upon cessation of shear flow. At very low shear rates, Dixon *et al.*⁹ found single-exponential relaxation rates of the shear-enhanced light scattering intensity which followed the equilibrium dynamics of the concentration fluctuations. These equilibrium dynamics are described by a two-fluid model of Brochard and de Gennes²⁹ in which the relaxation time is the sum of two processes: a q -independent stress relaxation component and a q -dependent diffusive component:

$$\tau(q) = \tau_s + \frac{1}{Dq^2} \quad (7)$$

where D is the cooperative diffusion coefficient for concentration fluctuations and τ_s is the stress relaxation

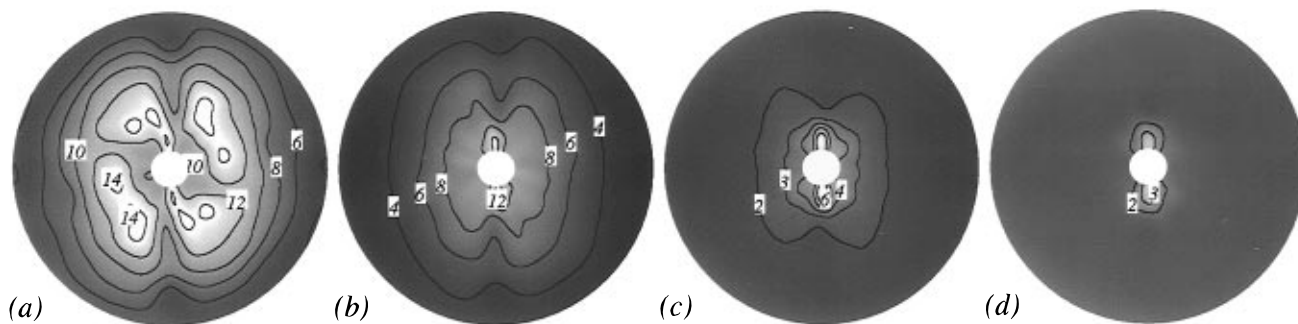


Figure 10. $S(q_x, q_y, t)$ for several times after the cessation of shear flow: (a) 1.0 s; (b) 2.0 s; (c) 10 s; (d) 30 s. The structure factor just prior to the cessation of shear flow is shown in Figure 8d.

time. At moderate shear rates van Egmond *et al.*¹² and Dixon *et al.*³⁰ reported a two-stage relaxation process. Both groups observed a rapid elastic response in which the entire two-dimensional scattering pattern in the shear plane, $S(q_x, q_y, t)$, shifted in a manner which represented a small reversal of the shear flow. They attributed this reversal to stored elastic energy in their polymer solutions. This rapid elastic response was followed by a slower decay which became increasingly nonexponential as the shear rate increased. Nevertheless, at moderate shear rates, the slowest relaxation was well described by eq 7.

Nakatani *et al.*³¹ also measured the relaxation dynamics at moderate-to-high shear rates, but in the velocity–vorticity (q_x – q_z) plane. They found behavior similar to that described above. They observed a very rapid response followed by a slower q -dependent exponential relaxation back to equilibrium which could be characterized by an equilibrium collective diffusion coefficient. In contrast to the observations of van Egmond *et al.*¹² and Dixon *et al.*,³⁰ they found that the anisotropy of the scattering pattern in the velocity–vorticity plane disappeared completely in the rapid relaxation phase.

Returning to the data obtained in this study, we note that when $\dot{\gamma}$ exceeds $\dot{\gamma}_c$, the scattering pattern remains anisotropic for the full relaxation period and, more importantly, the relaxation times become very much longer than those observed below $\dot{\gamma}_c$. Closer examination of the relaxation of the full structure factor reveals important properties not apparent in Figure 7b. In Figure 10, we show the evolution of the structure factor upon cessation of shear after the sample has been sheared for 45 s at a shear rate of $\dot{\gamma} = 90 \text{ s}^{-1}$; the structure factor just prior to the cessation of shear is shown in Figure 8d. One striking feature of these plots is that while it takes a very long time for the structure factor to relax back to its equilibrium state, it very rapidly becomes symmetric with respect to the q_y axis. One second after the cessation of shear flow, the scattering pattern (Figure 10a) shows only a small remnant of asymmetry; after 2 s, no measurable asymmetry remains (Figure 10b). Thus, the symmetric part of the scattering we identified in Figure 8 exhibits a much slower decay than does the antisymmetric part. In fact, to within the accuracy of our data, the antisymmetric part of the structure factor decays at the same rate above and below the critical shear rate $\dot{\gamma}_c$ and is consistent with the dynamics described by eq 7 as were the previous studies of Dixon *et al.*^{9,30} and van Egmond *et al.*¹² This is an important indication that the symmetric part of the structure factor represents a qualitatively new feature characteristic of the highly sheared state.

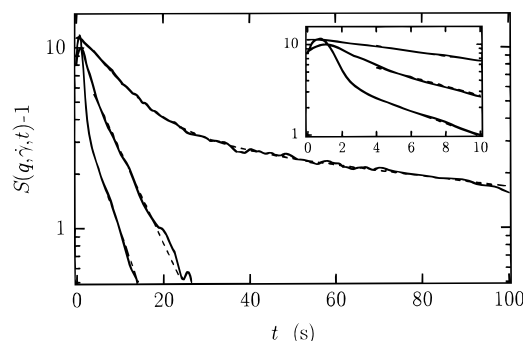


Figure 11. $S(\mathbf{q}, \dot{\gamma}, t)$ for selected \mathbf{q} after the cessation of shear flow corresponding to $\dot{\gamma} = 90 \text{ s}^{-1}$. The inset shows the elastic response and fast decay of the antisymmetric mode in the first 2 s after the cessation of shear flow. The two faster decaying curves are characteristic of the relaxation of light scattering away from the origin along the q_y axis. After the initial elastic transient, they exhibit single exponential behavior with decay times of 6.2 s ($q_x = 10.6 \mu\text{m}^{-1}$, $q_y = 10.6 \mu\text{m}^{-1}$) and 8.4 s ($q_x = 5.0 \mu\text{m}^{-1}$, $q_y = 0.0 \mu\text{m}^{-1}$), respectively. The more slowly decaying curve was taken for $q_x = 0.4 \mu\text{m}^{-1}$, $q_y = 5.0 \mu\text{m}^{-1}$, and $q_z = 0 \mu\text{m}^{-1}$ and is well-described by a double exponential with decay times of 6.2 and 130 s.

Another compelling indication of how far the system has been driven from its equilibrium state is the relaxation behavior of the static structure factor at very small q . Except at small wavevectors along the q_y -axis, the entire scattering pattern shown in Figure 10 relaxes with a time constant of between 6 and 10 s, with only a weak q dependence. For small wavevectors along the q_y -axis, however, strong scattering persists much longer, and relaxes only after several minutes. This can be seen in Figure 11 where we plot $S(q) - 1$ as a function of time (recall that we have defined the equilibrium value of $S(q)$ to be unity) for three representative points in \mathbf{q} space. The data show that after an initial transient elastic response lasting a couple of seconds, the data decay monotonically. With the exception of the data taken at small q along the q_y -axis, the data at all \mathbf{q} decays as a single exponential. The time constant of the decay is 5–10 s, with the data taken at smaller q having a somewhat slower decay than the data taken at larger q . The decay of the light scattering data along the q_y -axis, however, is best described by a double exponential of the form $A_1 \exp(-t/\tau_1) + A_2 \exp(-t/\tau_2)$. The shorter time constant τ_1 is several seconds long, comparable to the relaxation times observed for the data off the q_y -axis. The longer time constant is at least several minutes long (its exact value is difficult to determine because of temporal fluctuations in the scattering and the long observation times required). We associate these very long relaxation times with the observed buildup of strong concentration fluctuations

over very large length scales ($\sim 2 \mu\text{m}$), as indicated by the small values of q_y where this behavior is observed. These long relaxation times suggest that the system has been driven very far from its equilibrium state and could be regarded as a signature of phase separation.

VIII. Is This Shear-Induced Phase Separation?

There have been many reports of shear-induced phase separation in semidilute polymer solutions near the equilibrium demixing phase boundary, *i.e.*, for semidilute Θ solutions. It is unclear, however, just exactly what is meant by a "phase transition" in this context, since the term is strictly defined only for a system in equilibrium; a system subjected to an imposed shear flow is, of course, *out of* equilibrium. For an equilibrium system, a first-order phase transition is associated with a discontinuous change in some observable property of the system, for example, a change in concentration for a polymer solution or a change in density for a gas-liquid transition. The kinetics of this transition are typically slow, being limited, for example, by mass or thermal transport. Frequently, two phases coexist in equilibrium with each other after having undergone a phase transition. Furthermore, a system that has undergone a first-order phase transition frequently exhibits hysteresis accompanied by very long relaxation times when the external constraints (*e.g.*, temperature, pressure, *etc.*) are returned to the single-phase regime.

In previous studies on semidilute Θ solutions, it was shown that weak shear flow does not produce an abrupt change in any known properties of the system. Moreover, there is no hysteresis and the relaxation times observed are characteristic of the equilibrium state.⁹ Nevertheless, it may be possible that an imposed shear continuously *shifts* the transition to higher temperatures, as is observed in simple binary liquid mixtures.^{32,33}

By contrast, for the experiments reported in this paper, there seems to be an abrupt change in several sample properties when the shear rate is increased beyond a *finite* critical shear rate $\dot{\gamma}_c$ of approximately 60 s^{-1} . Consider the changes we have observed when the shear rate is increased above 60 s^{-1} . Just below $\dot{\gamma}_c$ we observe two peaks in the structure factor occurring in the second and fourth quadrants. These peaks develop within a few seconds after the shear flow commences. By contrast, above $\dot{\gamma}_c$, we observe four peaks in the structure factor; these four peaks correspond to a new 4-fold symmetric mode which coarsens over a time scale lasting more than several minutes. Ultimately, the four-peak pattern develops into a pair of peaks along the gradient direction. These peaks correspond to layered structures with spacings on the order of $1 \mu\text{m}$. When the shear flow is turned off, the system returns to its equilibrium state, but again, the time scales over which this occurs are vastly different depending on whether or not the shear rate exceeds the critical shear rate $\dot{\gamma}_c$. For $\dot{\gamma} < \dot{\gamma}_c$, the system returns to equilibrium in less than 1 s. For $\dot{\gamma} > \dot{\gamma}_c$, the time for the system to return to equilibrium is very long and depends strongly on q . The relaxation at most q observed with light scattering exhibits decay times lasting many seconds. For small q along the q_y axis, the relaxation time is at least several minutes. Another indication that these phenomena might be well-described as a phase transition is the increase in scattering along the q_y axis, particularly at small q_y . The observed time dependence of this scattering also bears

at least a qualitative resemblance to scattering from a system undergoing phase separation via spinodal decomposition. Therefore, while we do not know of any rigorous criteria for phase transitions in a nonequilibrium system, the phenomena reported here seem consistent with a shear-induced phase transition.

IX. Conclusion

In these experiments we use light scattering to study the transient and steady state structures that develop in a semidilute polymer solution following initiation of simple shear flow. We find a qualitative change in the scattering behavior at a critical shear rate $\dot{\gamma}_c$ and interpret these results in terms of a phase separation. In particular, we have identified a new kind of shear-induced fluctuation, distinct from those described by the HF mechanism which we have discussed in terms of a possible shear-induced phase transition. While it is not rigorously clear what the experimental signature of a phase transition should be, there are several factors that argue in favor of this kind of description, as outlined above. We wish to emphasize the observed separation in time scales between the shear-induced concentration fluctuations (as seen at early times) and the coarsening (observed at later times) which indicates that different physical mechanisms are involved. We identify the first mechanism as the HF effect and the second as a shear-induced phase separation. The coarsening behavior described above corresponds to the formation and growth of these domains. However, the domains are still under shear; thus the HF mechanism of enhanced concentration fluctuations in a sheared single-phase polymer solution still applies to these domains. This explains the observation that the HF mechanism persists at shear rates above $\dot{\gamma}_c$.

Acknowledgment. We wish to thank Paul Dixon for several valuable discussions.

References and Notes

- (1) Rangel-Nafaile, C.; Metzner, A.; Wissbrun, K. *Macromolecules* **1984**, *17*, 1187.
- (2) Larson, R. *Rheol. Acta* **1992**, *31*, 497.
- (3) Helfand, E.; Fredrickson, G. *Phys. Rev. Lett.* **1989**, *62*, 2468.
- (4) Milner, S. *Phys. Rev. E* **1993**, *48*, 3674.
- (5) Onuki, A. *J. Phys. Soc. Jpn.* **1990**, *59*, 3423.
- (6) Doi, M. *Polym. Prepr. Jpn.* **1990**, *39*, 1260.
- (7) Ji, H.; Helfand, E. *Macromolecules* **1995**, *28*, 3869.
- (8) Wu, X.-l.; Pine, D.; Dixon, P. *Phys. Rev. Lett.* **1991**, *66*, 2408.
- (9) Dixon, P.; Pine, D.; Wu, X.-l. *Phys. Rev. Lett.* **1992**, *68*, 2239.
- (10) Moldenaers, P.; Yanase, H.; Mewis, J.; Fuller, G. G.; Lee, C.-S.; Magda, J. J. *Rheol. Acta* **1993**, *32*, 1.
- (11) Yanase, H.; Moldenaers, P.; Mewis, J.; Abetz, V.; van Egmond, J.; Fuller, G. G. *Rheol. Acta* **1991**, *30*, 89.
- (12) van Egmond, J.; Werner, D.; Fuller, G. *J. Chem. Phys.* **1992**, *96*, 7742.
- (13) van Egmond, J.; Fuller, G. *Macromolecules* **1993**, *26*, 7182.
- (14) Hashimoto, T.; Fujioka, K. *J. Phys. Soc. Jpn.* **1991**, *60*, 356.
- (15) Hashimoto, T.; Kume, T. *J. Phys. Soc. Jpn.* **1992**, *61*, 1839.
- (16) Moses, E.; Kume, T.; Hashimoto, T. *Phys. Rev. Lett.* **1994**, *72*, 2037.
- (17) Kishbaugh, A.; McHugh, A. *Rheol. Acta* **1993**, *32*, 9.
- (18) Kishbaugh, A.; McHugh, A. *Rheol. Acta* **1993**, *32*, 115.
- (19) Nakatani, A.; Douglas, J.; Han, C. *J. Chem. Phys.* **1994**, *100*, 3224.
- (20) Hammouda, B.; Nakatani, A. I.; Waldow, D. A.; Han, C. C. *Macromolecules* **1992**, *25*, 2903.
- (21) Boue, F.; Lindner, P. *Europhys. Lett.* **1994**, *25*, 421.
- (22) VerStrate, G.; Philippoff, W. J. *J. Polym. Sci., Polym. Lett. Ed.* **1974**, *12*, 267.
- (23) Certain equipment and instruments or materials are identified in this paper in order to adequately specify the experimental conditions. Such identification does not imply rec-

- ommendation by the National Institute of Standards and Technology, nor does it imply that the materials are necessarily the best available for the purpose.
- (24) Pearson, D.; Herbolzheimer, E.; Grizzuti, N.; Marrucci, G. *J. Polym. Sci. B* **1991**, *29*, 1589.
- (25) Mani, S.; Malone, M.; Winter, H.; Halary, J.; Monerie, L. *Macromolecules* **1991**, *24*, 5451.
- (26) Mani, S.; Malone, M.; Winter, H. *Macromolecules* **1992**, *25*, 5671.
- (27) Laufer, Z.; Jalink, H.; Staverman, J. *J. Polym. Sci., Polym. Chem.* **1973**, *11*, 3005.
- (28) Magda, J.; Lee, C.; Muller, S.; Larson, R. *Macromolecules* **1993**, *26*, 1696.
- (29) Brochard, F.; de Gennes, P.-G. *Macromolecules* **1977**, *10*, 1157.
- (30) Dixon, P.; Pine, D.; Wu, X.-I. In *Complex Fluids*; Materials Research Society: Pittsburgh, PA, 1992; pp 127-138.
- (31) Nakatani, A. I.; Waldow, D. A.; Han, C. C. *Polym. Mater. Sci. Eng.* **1991**, *65*, 216.
- (32) Onuki, A.; Kawasaki, K. *Ann. Phys.* **1979**, *121*, 456.
- (33) Beysens, D.; Gbadamassi, M.; Moncef-Bouanz, B. *Phys. Rev. A* **1983**, *28*, 2491.

MA9510092